Biosensors and Bioelectronics 35 (2012) 167–173

Contents lists available at SciVerse ScienceDirect

Biosensors and Bioelectronics

journal homepage: www.elsevier.com/locate/bios

Label-free reflectometric interference microchip biosensor based on nanoporous alumina for detection of circulating tumour cells

Tushar Kumeria[a,b], Mahaveer D. Kurkuri[a,b], Kerrilyn R. Diener[c,d], Luke Parkinson[a], Dusan Losic[a,b,*]

[a] Ian Wark Research Institute, University of South Australia, Mawson Lakes, SA 5095, Australia
[b] School of Chemical Engineering, University of Adelaide, SA 5005, Australia
[c] Experimental Therapeutics Laboratory, Hanson Institute, Royal Adelaide Hospital, Adelaide, SA 5000, Australia
[d] School of Paediatrics and Reproductive Health, The University of Adelaide, Adelaide, SA 5005, Australia

ARTICLE INFO

Article history:
Received 4 December 2011
Received in revised form 9 February 2012
Accepted 17 February 2012
Available online 25 February 2012

Keywords:
Reflectometric interference spectroscopy
Optical biosensor
Label-free biosensor
Nanoporous alumina
Circulating tumour cells

ABSTRACT

In this report, a label-free reflectometric interference spectroscopy (RIfS) based microchip biosensor for the detection of circulating tumour cells (CTCs) is demonstrated. Highly ordered nanoporous anodic aluminium oxide (AAO) fabricated by electrochemical anodization of aluminium foil was used as the RIfS sensing platform. Biotinylated anti-EpCAM antibody that specifically binds to human cancer cells of epithelial origin such as pancreatic cancer cells (PANC-1) was covalently attached to the AAO surface through multiple surface functionalization steps. Whole blood or phosphate buffer saline spiked with low numbers of pancreatic cancer cells were successfully detected by specially designed microfluidic device incorporating an AAO RIfS sensor, without labour intensive fluorescence labelling and/or pre-enhancement process. Our results show that the developed device is capable of selectively detecting of cancer cells, within a concentrations range of 1000–100,000 cells/mL, with a detection limit of <1000 cells/mL, a response time of <5 min and sample volume of 50 μL of. The presented RIfS method shows considerable promise for translation to a rapid and cost-effective point-of-care diagnostic device for the detection of CTCs in patients with metastatic cancer.

1. Introduction

Cancer accounts for up to 15% (~8 million) of total deaths worldwide (Jemal et al., 2011; Msaouel and Koutsilieris, 2011), most as a result of metastatic disease. Metastatic disease occurs as a result of cancer cells from the primary tumour disseminating into the bloodstream and forming new tumours in various peripheral locations. These disseminated tumour cells are known as circulating tumour cells (CTCs) and have been most often observed in patients with disease of epithelial origin, such as pancreatic, melanoma and bladder cancer. The detection and quantification of CTCs in blood specially during the initial stages of metastatic disease are particularly important in diagnosis, monitoring and treatment of cancer diseases (Chambers et al., 2002; de Bono et al., 2008).

The major challenge in to detect a small number of CTCs in blood, since even for patients at an advanced stage of metastasis, the CTCs counts may only be few tens to thousands per millilitre of blood, which also contains millions of leukocytes and billions of erythrocytes (Allard et al., 2004; Fan et al., 2009). Recent developments have been mainly focused for sorting and enumerating CTCs from blood samples, using density gradients (Baker et al., 2003), size filtration (Vona et al., 2000; Zheng et al., 2007), immunomagnetic separation/isolation (Benez et al., 1999; Talasaza et al., 2008), dielectrophoresis (DEP) (Gascoyne et al., 2009), and immunochemistry coupled with specific microfluidic designs using micropillars (Nagrath et al., 2007; Kurkuri et al., 2011) and nanostructured surfaces (Wang et al., 2009). After the enrichment process, most of these systems necessitate the challenge of subsequent CTCs identification using techniques such as flow cytometry and fluorescence microscopy, which are labour-intensive and time consuming. To address these limitations, a label-free biosensing of CTCs for direct detection and measurement of CTCs without enrichment and separation steps is a desirable attractive solution. Several label-free biosensing technologies have been reported for the detection and monitoring of live CTCs including: electrochemical impedance (Weng et al., 2011; Li et al., 2010), quartz crystal microbalance (Zhou et al., 2000; Pan et al., 2010), surface plasmon resonance spectroscopy (Myung et al., 2011), optical waveguide light mode spectroscopy (Ramsden et al., 1995; Fang, 2007) and immunomagnetic biosensing coupled with impedemetric method (Chung et al., 2011). The detection capabilities of these techniques are summarised in Table 1S (Supplementary Information). In current trends of point-of-care type of diagnostics where micro-chip device is

* Corresponding author at: School of Chemical Engineering, University of Adelaide, SA 5005, Australia. Tel.: +61 (0) 8 8313 4648; fax: +61 (0) 8 8313 4373.
E-mail address: dusan.losic@adelaide.edu.au (D. Losic).

0956-5663/$ – see front matter.
doi:10.1016/j.bios.2012.02.038

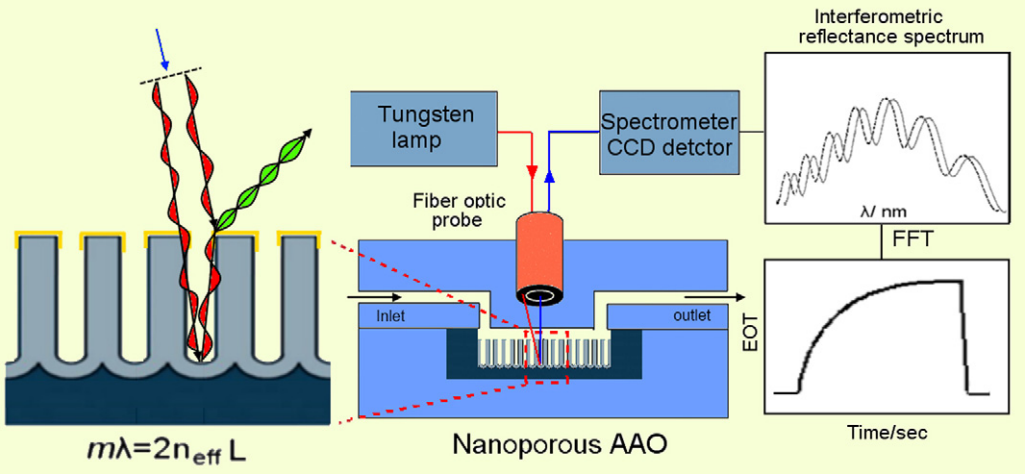

Fig. 1. Schematic of the RIfS microchip detection system: comprising a AAO nanopore as sensing platform integrated into a microfluidic chip, fiber optic probe connected to a light source and CCD detector. The interaction of light with the pore structures generates a Fabry–Perot interference pattern and the shift of fringe pattern as result of binding molecules or cells on the AAO surface is resolved into Effective Optical Thickness (EOT/nm) by applying Fast Fourier Transform (FFT) analysis and used as detection signal.

integrated system, it is essential that the detection system is compatible with microfluidic systems, provides non-invasive label-free detection, ultra-high sensitivity and selectivity, fast response times and has the ability to work with nano or sub microlitre volumes (Marko-Varga et al., 2003). The Reflectometric interference spectroscopy (RIfS) which addresses the most of these requirements is a particularly promising detection method for biosensing (Gauglitz, 2005).

The RIfS is an optical method based upon interference between incident and reflected light beams derived from the upper and lower surfaces of a thin film or structure with well-defined nanotopography (Gauglitz, 2005, 2010). This technique has been applied for the detection of various biological entities such as DNA and proteins initially using planar polymer films and recently nanostructured substrates, including porous silicon, aluminium oxide (AAO) and titania nanotube arrays (Alvarez et al., 2009a,b; Lin et al., 1997; Mun et al., 2010). Nanoporous AAO fabricated by electrochemical anodization of Al is an inexpensive, simple to produce, have highly ordered 3-dimensional (3-d) pore structures with a high surface area for increased ligand immobilization (Losic et al., 2011). Furthermore, AAO is mechanically, chemically and thermally stable, easy to functionalize, and yields a very strong interference pattern which makes it one of the most promising substrates for RIfS sensing (Losic et al., 2008, 2011; Jani et al., 2010; Kumeria et al., 2011; Kumeria and Losic, 2011, 2012). A schematic RIfS interferometric microchip sensor showing the interaction of light with AAO pore structure and generation of RIfS signal is presented in Fig. 1.

Reflection of white light at the top and bottom of the AAO porous layer results in a characteristic interference pattern with Fabry–Perot fringes, which are dependent on the product of refractive index and the film thickness, giving rise to an effective optical thickness (EOT: $2n_{eff}L$) which is sensitive to subtle changes in refractive index of the porous structure caused by the binding of molecules on the surface.

In this study, we demonstrate for the first time, the application of a label-free microchip biosensing device for the detection of CTCs based on RIfS on nanoporous AAO. Biotinylated anti-EpCAM antibody that binds to human carcinoma cells overexpressing the epithelial cell adhesion molecule (EpCAM) was covalently attached to the modified AAO surface and used as a CTCs capturing platform as illustrated in Fig. 2. The binding of CTCs on the antibody modified AAO surface is proposed to provide a strong influence on the RIfS signal causing a wavelength shift in the Fabry–Perot interference fringes, and therefore applied for CTCs detection.

Self-assembled monolayers (SAM) of mercaptoundecanoic acid (MUA) with a long carbon chain was selected for the functionalization of gold coated AAO to provide the appropriate carboxylic acid terminal group for subsequent streptavidin–biotin antibody attachment, a softer binding surface for cancer cells and prevent non-specific cell binding by electrostatic repulsion (Losic et al., 2001). The performance of the developed RIfS sensing device system was characterized by using anti-EpCAM and non-anti-EpCAM binding cells.

2. Materials and methods

2.1. Materials

Aluminium foil (0.1 mm, 99.997%) was supplied by Alfa Aesar (USA). Oxalic acid, ethanol (Chem Supply, Australia), chromium trioxide (Mallinckrodt, USA), 11-mercaptoundecanoic acid (MUA), *N*-Hydroxysuccinimide (NHS), ethyl(dimethylaminopropyl) carbodiimide (EDC), ethanolamine, streptavidin (Sigma–Aldrich, Australia), and biotinylated antibodies (eBioscience, San Diego, CA, USA) were used as received. Milli Q (Millipore, USA) water was used for preparation of all solutions followed with a final filtering through a 0.22 μm filter.

2.2. Preparation of nanoporous anodic aluminium oxide (AAO)

AAO substrates were prepared by two-step electrochemical anodization of Al foil (10 mm × 10 mm) in a 0.3 M oxalic acid at 0 °C as described previously (Masuda and Fukuda, 1995; Losic and Lillo, 2009; Kumeria and Losic, 2012). First anodization was carried out at voltage between 50 and 60 V to form an initial porous alumina layer, that was removed by dipping in oxide removal solution (0.2 M chromium trioxide and 0.4 M phosphoric acid) for 1–2 h at 60 °C. After removal of the first layer, textured aluminium foil was subjected to the final anodization, that was carried out at 50 V for 40 min under the same conditions. This anodization process yielded AAO layer with pores of 32 ± 3 nm diameter and depths of 4 ± 0.2 μm which satisfies all mathematical and structural requirements for generating intense reflective interference spectrum.

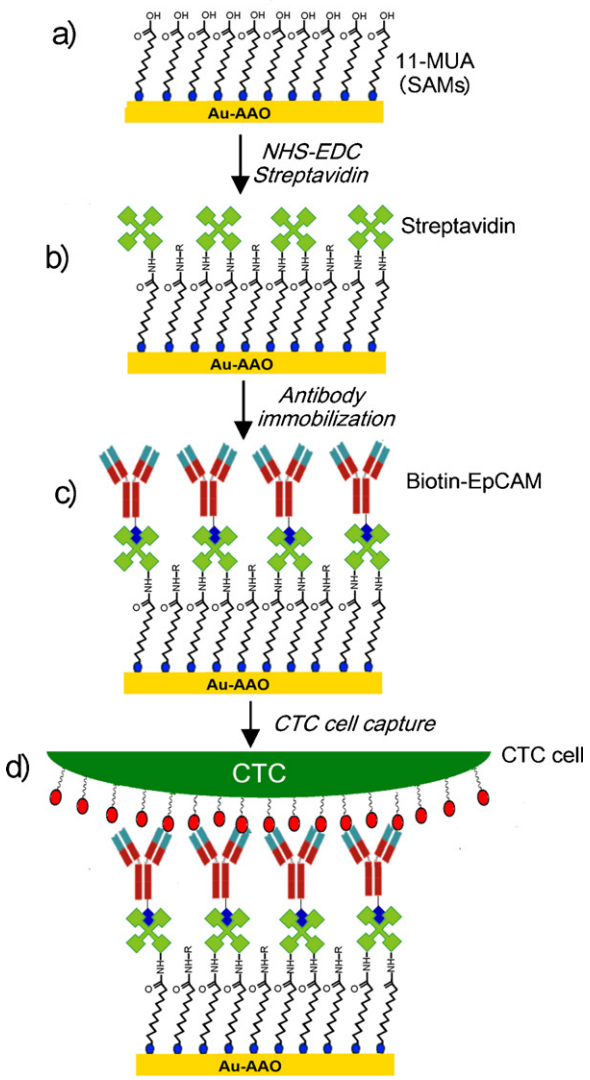

Fig. 2. Schematic illustration of the surface functionalization steps of gold modified AAO used for RIfS biosensing which involves (a) the formation of self-assembled monolayers (SAMs) of carboxyl-containing thiol followed by (b) covalent attachment of streptavidin on activated SAMs after activation with coupling (NHS/EDC) agents and finally (c) immobilization of biotinylated Anti-EpCAM antibodies; (d) scheme of binding of CTC cell on anti-EpCAM antibodies.

2.3. Immobilization of anti-EpCAM antibodies on AAO

Ultra-thin (~8 nm) metal films of Au were deposited on to AAO by metal vapour deposition instrument (Emitech K975X, UK). The thickness of the deposited film was controlled by the in-built quartz crystal film thickness monitor. The anti-EpCAM antibody functionalization of Au coated AAO was performed using a series of modifications steps illustrated in Fig. 2. The Au-AAO samples were cut into 5 mm × 5 mm size followed by immersing in a 10 mM solution of MUA in ethanol overnight to form densely packed SAMs (MUA-Au-AAO) on their surface followed by washing with ethanol and ultra pure water. A freshly prepared 1:1 mixture of NHS (0.1 M) and EDC (0.1 M) aqueous solution (Su et al., 2005) was then added onto the sample surface for 7 min to activate the free carboxyl groups followed by washing with acetate buffer (pH 5). The streptavidin at 100 μg/mL concentration in acetate buffer was then added for 1 h allowing for its covalent bonding to the MUA. Samples then were subsequently rinsed with milli Q water and PBS solution, followed by the addition of 1 M ethanolamine–HCl for 10 min to block the remaining activated carboxyl groups. The streptavidin modified AAO was finally incubated with 50 μg/mL biotinylated anti-EpCAM antibody or biotinylated isotype control antibody diluted in PBS for 30 min followed by rinsing with PBS solution and used immediately after preparation or stored in PBS in fridge to prevent them from drying.

2.4. Microfluidic device fabrication and assembly of RIfS biosensor

The microfluidic device was fabricated in two re-useable halves and sealed during use by fixing in a bondless microfluidic device clamp for hybrid materials (ANFF-SA, South Australia) (Kumeria and Losic, 2011). The microstructures were formed in solid poly-(methyl methacrylate) (PMMA) by the hot-embossing process using a brass stamp, machined by CNC micromachining (Supermill-2M, Kira), at 4.3 MPa at 130 °C using a hot embosser-substrate bonder (EVG, 520-HE). The microfluidic structure integrated two channels with simple mixers in order to evenly distribute fluid delivery to a cavity which accommodated a AAO sensing platform, leaving a further 100 μm space between the substrate and borosilicate glass lid where fluid could pass, forcing all cells to pass in close proximity over the top of the functionalized AAO surface (Fig. 3).

The device clamp also facilitated integration of the spectrophotometer probe to a well-defined position above the substrate.

2.5. Cell sample preparation

The EpCAM-positive pancreatic tumour cell line, PANC-1, was cultured in Roswell Park Memorial Institute (RPMI), media supplemented with 10% heat-inactivated foetal calf serum, 100 U/mL penicillin and gentamycin, 2 mM L-glutamine and 10 mM HEPES. Cells were subsequently harvested by incubation in TrypLE™ dissociation solution (Invitrogen) for 5 min at 37 °C. Resultant cells were washed in endotoxin-free PBS, and a 30 μL sample diluted 1:2 with the trypan blue exclusion dye for counting on a standard haemocytometer to determine viable cell concentration. Cells were resuspended at the appropriate concentration prior to further use. Jurkat cells, a T cell leukaemia cell line, were similarly maintained and prepared as above, and were used as a non-EpCAM-expressing control cell line.

2.6. Characterization of AAO substrates

The pore diameters and thickness of the AAO before Au deposition were determined by scanning electron microscope (SEM) (FEI Quanta 450). For cross-sectional SEM imaging, free-standing AAO pores were prepared by removing the underlying Al using $CuCl_2$/HCl solution.

2.7. Microscopic verification of tumour cell attachment to AAO sensor

Images of CTCs bound to the AAO surface functionalized with biotinylated anti-EpCAM antibody were collected by OLYMPUS BH 2-UMA microscope integrated with a Moticam 2000 digital camera controlled by computer Motic Images Plus 2.0 software.

2.8. RIfS optical setup and detection of CTCs

A detailed description of the RIfS optical setup is provided in our previous work (Kumeria and Losic, 2011, 2012). Briefly, white light emerging from a bifurcated optical fibre probe bundle was incident at a spot of 1 mm to 2 mm in diameter onto the anti-EpCAM functionalized AAO chip from the vertical direction. The reflected light from same illuminated spot was coupled into the detection fibre optic probe in the same bundle and analysed using a micro CCD spectrometer (Jaz-Ocean Optics, USA). The RIfS spectra from

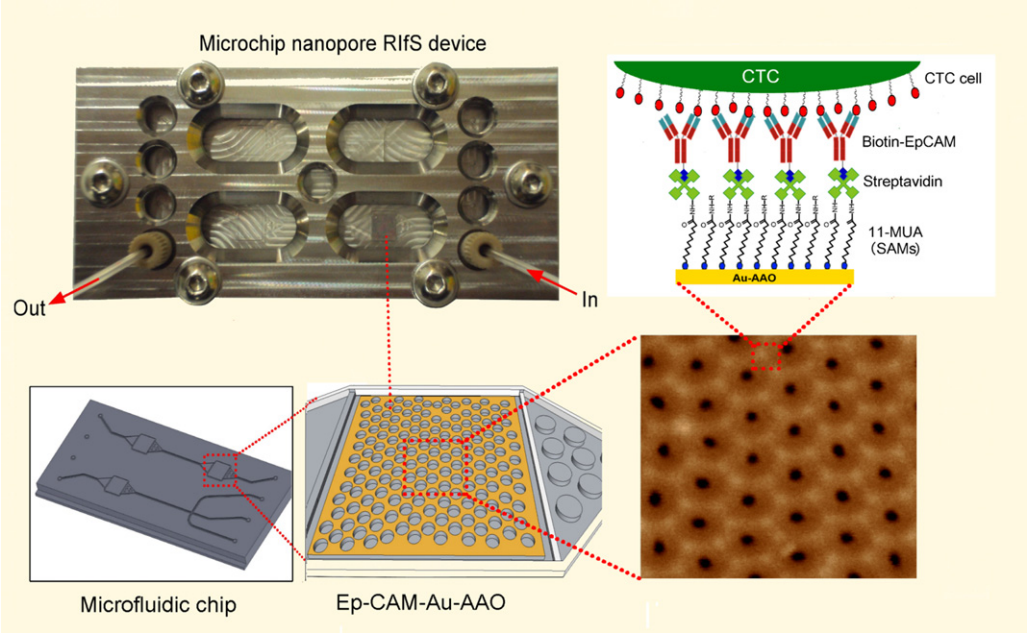

Fig. 3. The photo and schematic of microfluidic nanopore RIfS device composed of the embossing stamp with microfluidic channels (bottom left) and a AAO substrate (SEM image) (bottom right) modified with anti-EpCAM (top right) for capturing and detection of CTCs.

the anti-EpCAM-AAO sensor as a result of interaction with analyte were acquired in the 400–900 nm wavelength range. Spectral data were saved at intervals of 10 s with an integration time of 100 ms (averaging 5 measurements) followed by subsequent processing by Fast Fourier Transformation (FFT) from the Igor Pro library (Wavemetrics, USA), which allowed time-scaled measurements of CTCs capture. The changes of Effective Optical Thickness (Δ EOT) which provide sensitive information on changes to the optical path length due to changes in the refractive indices of the fluid medium and of the anti-EpCAM functionalized AAO interface ($2n_{eff}L$ value in the Fabry–Perot interference fringe equation) were plotted over time and used for the detection of CTCs.

The PANC-1 cells were spiked into the endotoxin-free PBS at concentrations of 1000; 5000; 10,000; 50,000; 100,000 and 200,000 cells/mL, and also in blood at 10,000 cells/mL. Total volume of 50 μL of samples with cells were injected into the device using a syringe pump without any prior enrichment at a flow rate of 6 μL/min for 5 min after attaining a stable baseline RIFs signal in PBS solution. After cell addition, washing with PBS was performed to remove unbound cells until a new and stable baseline of EOT value is obtained, leaving a signal that is purely due to specifically adsorbed CTCs. The EOT signals were obtained for each concentration of CTCs in solution using at least 3 anti-EpCAM–Au-AAO sensors. It is known that the hydrodynamics within the microfluidic channel impacts heavily on the ability of CTCs to attach to surface antibodies, through limitation of reaction time for antibody/target-molecule conjugation at high flow rates, or removal of bound cells through hydrodynamic shear, which exceeds the bond strength of the conjugate. Without performing a complicated analysis to this end, we briefly explored the influence of two different flow rates (6 μL/min and 12 μL/min) and two cell concentrations (1000 cells/mL and 100,000 cells/mL) that were likely to be suitable for the attachment of cells to our sensor.

Comparative studies using a non-EpCAM-expressing Jurkat cells (100,000 cells/mL) as control which do not bind to the Anti-EpCAM antibody on the CTCs sensitive AAO sensor surface and using PANC-1 cells (100,000 cells/mL) on isotype antibody modified AAO sensor surface were performed.

3. Results and discussions

3.1. Characterization of nanoporous aluminium oxide (AAO) structure and RIfS response

The diameter and length of pores in the AAO substrate critically determine its RIfS properties, therefore SEM characterization was performed to confirm the pore dimensions, which we have previously determined to have optimal optical performance (Kumeria and Losic, 2012). SEM images showing the top surface and cross-sectional structures of a representative AAO sample are presented in Fig. 4. These images confirm the typical AAO structure, with highly ordered pores organized in a hexagonal pattern (Fig. 4a) with perfectly straight, vertical pores closed at the bottom part by an oxide barrier layer (Fig. 4b). The structural parameters for the AAO used in this study (pore diameter = 32 ± 3 nm, pore length = 4 ± 0.2 μm) were in accordance with applied fabrication protocol to satisfy the mathematical requirements for generating a strong Fabry–Perot interference pattern (Kumeria and Losic, 2012). SEM images also confirmed that the gold coating and subsequent surface modification of AAO did not significantly change these pore structures (data not shown).

The typical RIfS response of the anti-EpCAM–Au-AAO microchip sensor, is presented as an interference pattern with Fabry–Perot fringes collected during the flow of PBS buffer solution through the microfluidic device is shown in Fig. 5a (red graph). (For interpretation of the references to colour in this figure legend, the reader is referred to the web version of the article.) The interference graph shows a large number of fringes (11) and high intensity, which are desirable optical characteristics for RIfS sensing. Both the intensity of fringe signals and the wavelength shift of the fringe pattern can be used for the detection of surface binding events including small molecules or large objects as cells. In the case of the CTCs detection, the wavelength shift of the interference signal was found to be most sensitive and therefore adopted for this work (Fig. 5a). The red shift of the RIfS signal (15 nm) after injection of 50 μL with 50,000 cells/mL PANC-1 cells in PBS provided initial confirmation of the ability of the anti-EpCAM–Au-AAO sensing device to detect the surface binding of CTCs. Fourier transformation of the interference

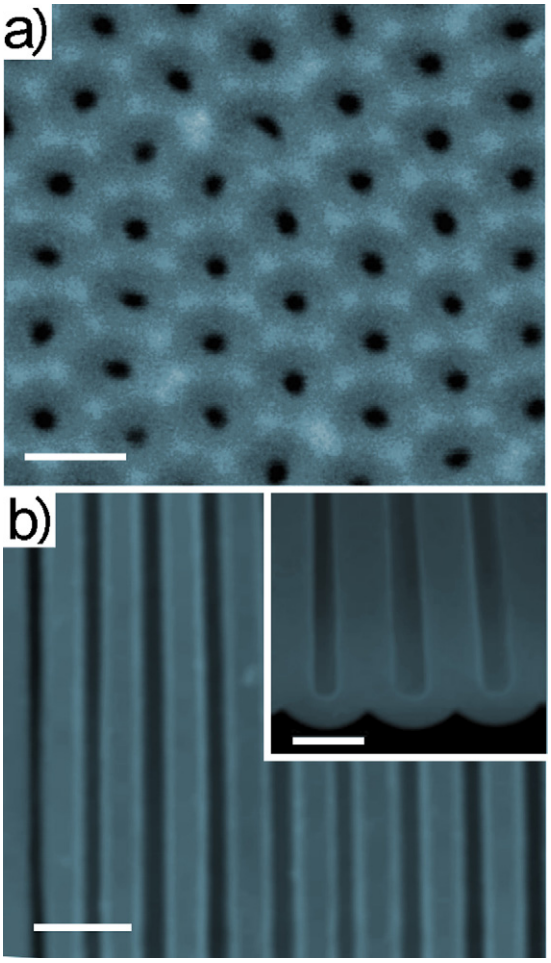

Fig. 4. SEM images of prepared AAO substrate (a) the top of AAO surface showing the pore size and their organization and (b) cross-sectional structure showing straight and vertically oriented pore structure. The inset is a bottom part of AAO with closed pores where underlying Al is removed for imaging purposes. The bar scale is 200 nm.

spectra enabled rapid conversion of data to effective optical thickness, which could be continuously monitored and presented as analytical ΔEOT versus time and interpreted as CTCs concentration vs time.

3.2. CTCs detection using RIfS on anti-EpCAM modified AAO

Fig. 5b shows the processed RIfS response (ΔEOT) from the anti-EpCAM–Au-AAO sensor after injection of 50,000 cells/mL PANC-1 cells in PBS. A significant and immediate increase of the EOT signal from the stable baseline was observed confirming the binding of tumour cells onto sensor surface was detected by RIfS system. An average response time to reach the 90% of the peak value was determined to be approximately 300 ± 30 s measured for each of the different CTC concentrations. The EOT signal increased only slightly over 5 min of continuous introduction of CTCs containing solution into the device. This indicated that most of the concentration-dependent capture of tumour cells occurred over this short time with subsequent increases due to steady occupation of remaining antibody binding sites. Hence, the measurements were limited to 5 min. Upon rinsing with PBS buffer, we observed that the signal was only slightly reduced to form a new base line. This suggests that the captured cells remained attached to the surface and the slight reduction in signal is due to the removal of non-bound cells and reflects the specificity of the functionalized sensor.

The calibration graph obtained from the testing of at least 4 sensing devices for CTCs (PANC-1) samples in the concentration range of 1000–200,000 cells/mL is presented in Fig. 5c. The degree of EOT shift recorded during 5 min of injection of cell-laden solution correlated strongly with the cellular concentration. A linear relationship between the CTCs concentration and ΔEOT was observed over the concentration range of 1000–10,000 cells/mL. The response and calibration graph appeared saturated (Fig. 5c) for cell concentrations above 100,000 cells/mL. This likely reflects a saturation of the sensor surface by attaching number of tumour cells, by either geometric exclusion or complete occupation of all anti-EpCAM–Au-AAO binding sites. The linear response with the detection limit of <1000 cells/mL was observed at lower concentrations of CTCs, that is valuable for practical applications as given the low number of CTCs present in blood which is relevant in clinical diagnosis. The large shift in EOT signal observed in our experiments suggests that with enhancements in microfluidic design beyond this rudimentary proof-of-concept example, a higher percentage of cells in low CTCs concentration in solution may be interrogated by the functionalized surface of the sensor, or by increasing the time-frame of measurement. Further optimisation of the microfluidic design to increase the chance of cell-AAO sensor interaction, and some optical improvements by reducing the size of illumination spot may indeed permit the detection of a single captured cell.

The velocity of the cells and the hydrodynamic shear force imposed on them by the carrier fluid inside a micro-channel influences the cells' ability to conjugate with the antibodies and remain attached respectively (Nagrath et al., 2007; Plouffe et al., 2008). This was confirmed by our brief analysis, carried out to measure the influence of two different flow rates on the ability of our anti-EpCAM–Au-AAO RIfS sensor to detect the CTCs, with the infusion of two concentrations ($\leq$1000 and $\geq$100,000 cells/ml) of PANC-1 cell solutions at 6 μL/min and 12 μL/min. At the higher flow rate, the increase in EOT signal was significantly delayed and upon rinsing with buffer, the EOT value was restored to the original baseline value observed prior to the introduction of CTCs (Fig. S2, Supplementary data). When the lower flow rate is applied (6 μL/min) the EOT showed a slow rise indicating a gradual increase in the number of captured cells on the sensor surface, without the signal reverting to the baseline after buffer infusion at the same rate. This result confirms a strong and irreversible attachment of the PANC-1 cells to the antibodies on the AAO sensing surface, which is influenced by the specific shear stress exerted onto the cancer cells by the hydrodynamic force. Beyond the simple hydrodynamic evaluation of cell attachment at two flow rates, these data further support the specificity of the sensor for measurement the attachment of CTCs on the AAO surface, rather than presence of cells in the buffer solution.

After performing the CTCs detection experiments at 50,000 cells/mL in PBS, the AAO sensors were carefully removed from the microfluidic device and examined under a microscope. Images in Fig. 5d shows the presence of many PANC-1 cells attached on the surface which density correlate with the concentration of CTCs in solution. Microscopic examination of the sensor surfaces from control experiments, using AAO with biotinylated isotype antibody instead of anti-EpCAM revealed no evidence of attached cells (Fig. 5e). This confirms the specific capture of CTCs by the anti-EpCAM-functionalized sensor and provides further evidence that the origin of the change in EOT is due to the conjugation of cancer cells to the surface rather than simply their presence in solution. A video recording showing the process of capturing of CTCs on AAO sensor surface is presented in Supplementary data (SM1).

3.3. Control experiment

The selectivity of our sensing device was evaluated by performing two control experiments as described earlier. Firstly,

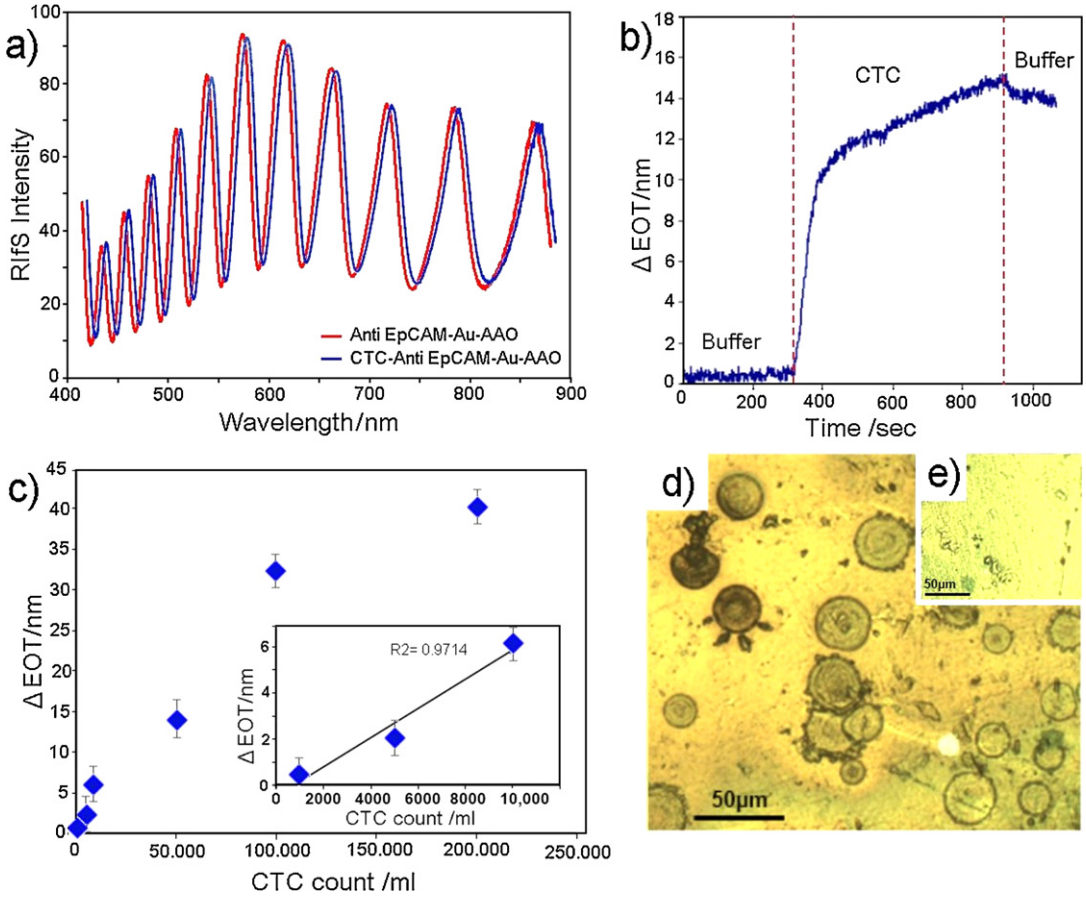

Fig. 5. (a) The shifting of the interference pattern of anti-EpCAM functionalized AAO sensor after introducing sample with 50,000 cells/mL (PANC-1) in PBS; (b) corresponding change in EOT over time, (c) a calibration curve showing the dependence of EOT signal as a function of CTCs concentration. The inset is the fitted linear analysis of EOT response for lower concentrations, (d) Light microscope images of the sensing surface after detection of CTCs with concentration of 50,000 cells/mL (PANC-1) showing number of cells attached on the surface; (e) Control surface of Au-AAO modified with isotype antibody that does not bind to CTCs under the same conditions showed no attached cells.

100,000 cells/mL cellular concentrations of the control non-EpCAM-expressing leukaemic cells (Jurkat cell line) were flowed under identical conditions over the sensors (Fig. S3a, Supplementary data). Only minor changes in EOT signal (<2 nm) were observed in comparison to the solution with same concentration of EpCAM-positive cancer cells, which caused a large shift in EOT (>32 nm). This difference is attributed to the fact that these control cells do not express EpCAM and therefore did not bind to the sensor surface. The minor signal shift observed for these cells was returned to the baseline after washing with buffer, indicating that it was due to either a non-specific adsorption of Jurkat cells to the sensor or due to the their presence in the carrier liquid. A second control experiment was performed using an isotype control antibody-functionalized sensor and infusing PANC-1 CTCs (100,000 cells/mL), again under identical conditions. The isotype antibody does not bind to EpCAM, or indeed any other human cell surface molecules, and therefore will not bind PANC-1 cells. As expected, minor and reversible changes in EOT (<1 nm) from baseline were observed (Fig. S3b, Supplementary data). Since, both of these control tests confirmed the selective binding of CTCs on the AAO sensor, which also showed good sensitivity, we were encouraged to determine its CTCs detection capability using a whole blood sample.

3.4. CTCs detection from blood sample

Finally, the sensitivity of our sensing device for the detection of CTCs (PANC-1 cells) from whole blood was investigated. Spiked blood samples were diluted (1 in 10) with PBS to overcome the possibility of agglomeration and coagulation of blood cells inside the microfluidic channel disrupting the flow of analyte. Two control experiments were carried out by flowing whole blood and blood spiked with EpCAM and non EpCAM expressing cells. After obtaining a stable baseline in PBS, the change in EOT signals were recorded for the injection of whole blood, blood + control non-EpCAM-expressing cells (Jurkat cells) (10,000 cells/mL), and blood + EpCAM-expressing pancreatic cancer cells (10,000 cells/mL) for a period of 5 min at 6 μL/min flow rate. The EOT signal was shifted by ~13 nm when the sensors were exposed to whole blood, or blood containing non-EpCAM binding cells. However, when the whole blood spiked with 10,000 PANC-1 cells/mL was infused through the device, a significantly greater EOT shift of 19 nm was observed (Fig. S4 Supplementary data). Whilst the CTC concentration was relatively high, these results clearly indicate the promising capabilities of the RIfS method using nanoporous AAO for the detection of CTCs in blood and suggest that further improvements are warranted.

4. Conclusion

A reflectometric interference label-free microchip biosensor based on nanoporous AAO for the detection of CTCs was demonstrated. The device is based on an inexpensive portable optical system integrated with AAO sensing platform functionalized with anti-EpCAM antibody, which specifically binds to CTCs, offering their capturing and detection in a single step. The presented device provides direct and a label-free detection of CTCs without of the

time-consuming analysis of capturing cells usually required for other methods. Results show the capability of measuring the concentration of cancer cells (1000–100,000 cells/mL) in PBS buffer solution including detection capability in diluted blood samples. The requirement of only small sample volumes (<50 μL) and complete measurements in less than 5 min are particularly attractive features of this method. Presented results indicate a good potential of developed device for clinical and point-of-care applications and further improvement with microfluidic and optical system design is proposed to lower detection limit (<10 cells).

Acknowledgements

This research was supported under Australian Research Council's (DP 0770930). We extended our thanks to Prof M.J. Sailor (UCSD) for his help providing FFT analysis software and to the ANFF-SA or the fabrication of the microfluidic device.

Appendix A. Supplementary data

Supplementary data associated with this article can be found, in the online version, at doi:10.1016/j.bios.2012.02.038.

References

Allard, W.J., Matera, J., Miller, M.C., Repollet, M., Connelly, M.C., Rao, C., Tibbe, A.G.J., Uhr, J.W., Terstappen, L.W.M.M., 2004. Clin. Cancer Res. 10, 6897–6904.
Alvarez, S.D., Derfus, A.M., Schwartz, M.P., Bhatia, S.N., Sailor, M.J., 2009a. Biomaterials 30, 26–34.
Alvarez, S.D., Li, C.-P., Chiang, C.E., Schuller, I.K., Sailor, M.J., 2009b. ACS Nano 3, 3301–3307.
Baker, M.K., Mikhitarian, K., Osta, W., Callahan, K., Hoda, R., Brescia, F., Kneuper-Hall, R., Mitas, M., Cole, D.J., Gillanders, W.E., 2003. Clin. Cancer Res. 9, 4865–4871.
Benez, A., Geiselhart, A., Handgretinger, R., Schiebel, U., Fierlbeck, G., 1999. J. Clin. Lab. Anal. 13, 229–233.
Chambers, A.F., Groom, A.C., MacDonald, I.C., 2002. Nat. Rev. 2, 563–572.
Chung, Y.-K., Reboud, J., Lee, K.C., Lim, H.M., Lim, P.Y., Wang, K.Y., Tang, K.C., Ji, H., Yu, M., Chen, Y., 2011. Biosens. Bioelectron. 26, 2520–2526.
de Bono, J.S., Scher, H.I., Montgomery, R.B., Parker, C., Miller, M.C., Tissing, H., Doyle, G.V., Terstappen, L.W., Pienta, K.J., Raghavan, D., 2008. Clin. Cancer Res. 14, 6302–6309.
Fan, T., Zhao, Q., Chen, J.J., Chen, W.T., Pearl, M.L., 2009. Gynecol. Oncol. 112, 185–191.
Fang, Y., 2007. Sensors 7, 2317–2329.
Gascoyne, P.R.C., Noshari, J., Anderson, T.J., Becker, F.F., 2009. Electrophoresis 30, 1388–1398.
Gauglitz, G., 2005. Anal. Bioanal. Chem. 381, 141–155.
Gauglitz, G., 2010. Anal. Bioanal. Chem. 398, 2363–2372.
Jani, A.M.M., Kempson, I.M., Losic, D., Voelcker, N.H., 2010. Angew. Chem. Int. Ed. 49, 7933–7937.
Jemal, A., Bray, F., Center, M.M., Ferlay, J., Ward, E., Forman, D., 2011. CA Cancer J. Clin. 61, 69–90.
Kurkuri, M.D., Al-Ejeh, F., Shi, J.Y., Palms, D., Prestidge, C., Griesser, H.J., Brown, M.P., Thierry, B., 2011. J. Mater. Chem. 21, 8841–8848.
Kumeria, T., Losic, D., 2012. Nanoscale Res. Lett. 7, 88.
Kumeria, T., Parkinson, L., Losic, D., 2011. Micro Nanosyst. 3, 290–295.
Kumeria, T., Losic, D., 2011. Phys. Status Solidi (RRL) 5, 406–408.
Li, T., Fan, Q., Liu, T., Zhu, X., Zhao, J., Li, G., 2010. Biosens. Bioelectron. 25, 2686–2689.
Lin, V.S.-Y., Motesharei, K., Dancil, K.-P.S., Sailor, M.J., Ghadiri, M.R., 1997. Science 278, 840–843.
Losic, D., Shapter, J.G., Gooding, J.J., 2001. Aust. J. Chem. 54, 643–648.
Losic, D., Lillo, M., 2009. Small 5, 1392–1397.
Losic, D., Velleman, L., Kant, K., Kumeria, T., Gulati, K., Shapter, J.G., Beattie, D.A., Simovic, S., 2011. Aust. J. Chem. 64, 294–301.
Losic, D., Cole, M.A., Dollmann, B., Vasilev, K., Griesser, H.J., 2008. Nanotechnology 19, 245704.
Marko-Varga, G., Nilsson, J., Laurell, T., 2003. Electrophoresis 24, 3521–3532.
Masuda, H., Fukuda, K., 1995. Science 268, 1466–1468.
Msaouel, P., Koutsilieris, M., 2011. BMC Cancer 11, 336–349.
Mun, K.-S., Alvarez, S.D., Choi, W.-Y., Sailor, M.J., 2010. ACS Nano 4, 2070–2076.
Myung, J.H., Gajjar, K.A., Pearson, R.M., Launiere, C.A., Eddington, D.T., Hong, S., 2011. Anal. Chem. 83, 1078–1083.
Nagrath, S., Sequist, L.V., Maheswaran, S., Bell, D.W., Irimia, D., Ulkus, L., Smith, M.R., Kwak, E.L., Digumarthy, S., Muzikansky, A., Ryan, P., Balis, U.J., Tompkins, R.G., Haber, D.A., Toner, M., 2007. Nature 450, 1235–1239.
Pan, Y., Guo, M., Nie, Z., Huang, Y., Pan, C., Zeng, K., Zhang, Y., Yao, S., 2010. Biosens. Bioelectron. 25, 1609–1614.
Plouffe, B.D., Radisic, M., Murthy, S.K., 2008. Lab Chip 8, 462–472.
Ramsden, J.J., Li, S.Y., Heinzle, E., Prenosil, J.E., 1995. Cytometry 19, 97–102.
Su, X., Wu, Y.J., Robelek, R., Knoll, W., 2005. Langmuir 21, 348–353.
Talasaza, A.H., Powellc, A.A., Huber, D.E., Berbeeb, J.G., Rohd, K., Yu, W., Xiao, W., Davis, M.M., Peasea, R.F., Mindrinos, M.N., Jeffrey, S.S., Davis, R.W., 2008. Proc. Natl. Acad. Sci. U.S.A. 196, 3970–3975.
Vona, G., Sabile, A., Louha, A., Sitruk, V., Romana, S., Schutze, K., Caproni,.F., Franco, D., Pazzagli, M., Vekemans, M., Lacour, B., Brechot, C., Paterlini-Brechot, P., 2000. Am. J. Pathol. 156, 57–63.
Wang, S., Wang, H., Jiao, J., Chen, K.J., Owens, G.E., Kamei, K., Sun, J., Sherman, D.J., Behrenbruch, C.P., Wu, H., 2009. Angew. Chem. Int. Ed. 121, 9132–9135.
Weng, J., Zhang, Z., Sun, L., Wang, J.A., 2011. Biosens. Bioelectron. 26, 1847–1852.
Zheng, S., Lin, H., Liu, J.Q., Balic, M., Datar, R., Cote, R.J., Tai, Y.C., 2007. J. Chromatogr. A 1162, 154–161.
Zhou, T., Marx, K.A., Warren, M., Schulze, H., Braunhut, S.J., 2000. Biotechnol. Prog. 16, 268–277.